Available online at www.sciencedirect.com
ScienceDirect
Deep-Sea Research I 54 (2007) 1402–1420
DEEP-SEA RESEARCH PART I
www.elsevier.com/locate/dsri

Meridional heat transport determined with expandable bathythermographs—Part II: South Atlantic transport

Silvia L. Garzoli*, Molly O. Baringer

NOAA Atlantic Oceanographic and Meteorological Laboratory, Miami, FL 33149, USA

Received 1 November 2006; received in revised form 9 April 2007; accepted 17 April 2007
Available online 29 April 2007

Abstract

Fourteen temperature sections collected between July 2002 and May 2006 are analyzed to obtain estimates of the meridional heat transport variability of the South Atlantic Ocean. The methodology proposed in Part I is used to calculate the heat transport from temperature data obtained from high-density XBT profiles taken along transects from Cape Town, South Africa to Buenos Aires, Argentina. Salinity is estimated from Argo profiles and CTD casts for each XBT temperature observation using statistical relationships between temperature, latitude, longitude, and salinity computed along constant-depth surfaces. Full-depth temperature/salinity profiles are obtained by extending the profiles to the bottom of the ocean using deep climatological data. The meridional transport is then determined by using the standard geostrophic method, applying NCEP-derived Ekman transports, and requiring that salt flux through the Bering Straits be conserved. The results from the analysis indicate a mean meridional heat transport of 0.54 PW (PW $= 10^{15}$ W) with a standard deviation of 0.11 PW. The geostrophic component of the heat flux has a marked annual cycle following the variability of the Brazil Malvinas Confluence Front, and the geostrophic annual cycle is 180° out of phase with the annual cycle observed in the Ekman fluxes. As a result, the total heat flux shows significant interannual variability with only a small annual cycle. Uncertainties due to different wind products and locations of the sections are independent of the methodology used.
Published by Elsevier Ltd.

Keywords: Heat transport

1. Introduction

Meridional heat transport in the ocean is a key element of the climate system because of the role that the ocean plays in determining the Earth's climate through its interaction with the atmosphere. In order to understand and predict climate variability, it is crucial to understand the mechanisms and the pathways of mass and heat transport in the global ocean. This oceanic meridional heat transport is due in part to a worldwide vigorous circulation that connects all the basins, the meridional overturning circulation (MOC). Despite its small size relative to the world ocean, the Atlantic Ocean is responsible for more than half of the northward heat transport carried by the global ocean. It is also the only ocean with northward heat

*Corresponding author. Tel.: +1 305 361 4338; fax: +1 305 361 4392.
E-mail addresses: Silvia.Garzoli@noaa.gov (S.L. Garzoli), Molly.Baringer@noaa.gov (M.O. Baringer).

0967-0637/$ - see front matter Published by Elsevier Ltd.
doi:10.1016/j.dsr.2007.04.013

transport across all latitudes (Talley, 2003). In the South Atlantic, the MOC is composed of northward transport of warm surface and intermediate layer waters in the upper 1200 m, southward transport of North Atlantic Deep Water between approximately 1200 and 4000 m, and northward flowing Antarctic Bottom Water below 4000 m (Talley, 2003). The South Atlantic Ocean interacts with the Pacific and the Indian Oceans. The meridional gaps between the continents of the Southern Hemisphere and Antarctica allow for a free exchange of water between the basins. The mean pathways of the South Atlantic circulation are fairly well known (e.g. Stramma and England, 1999). Gordon et al. (1992) concluded that the major proportion of the export of deep water from the North Atlantic is balanced by northward flow of lower thermocline and intermediate water through the South Atlantic Ocean, which is a local mixture of Indian and Pacific waters entering the basin as Agulhas Current leakage and through the Drake Passage, respectively.

Using data collected during the World Ocean Circulation Experiment (WOCE), Stramma and England (1999) examined the water mass distribution and circulation patterns in the South Atlantic. They organized the circulation into a layered scheme that can be summarized as follows (Fig. 1): the Deep Western Boundary Current (DWBC) transports North Atlantic Deep Water (NADW) from the northern hemisphere into the South Atlantic at depths between 1200 and 4000 m. The Antarctic Intermediate Water (AAIW) originates in the South Atlantic from a near surface region of the Circumpolar Current, especially in the Northern Drake Passage and the Malvinas Current Loop. AAIW from the Indian Ocean joins AAIW formed in the South Atlantic and South Pacific via the Agulhas leakage, and the resulting mix flows northward within the depth of the intermediate water layer (500–1200 m). South Atlantic Central Water (SACW) carried in the Brazil Current mixes with Indian Ocean Central Water brought into the Atlantic Ocean by the Agulhas Current intrusions. SACW flows in the upper layers between 100 and 500 m, following a more meridional pathway than the AAIW, as it transits from the eastern to western boundaries. Between 25° and 15°S, the flow moves meridionally next to the western boundary.

The upper ocean circulation in the southwestern Atlantic is characterized by the encounter between the relatively warm and salty southward-flowing Brazil Current and the relatively cold and fresh northward-flowing Malvinas Current. This

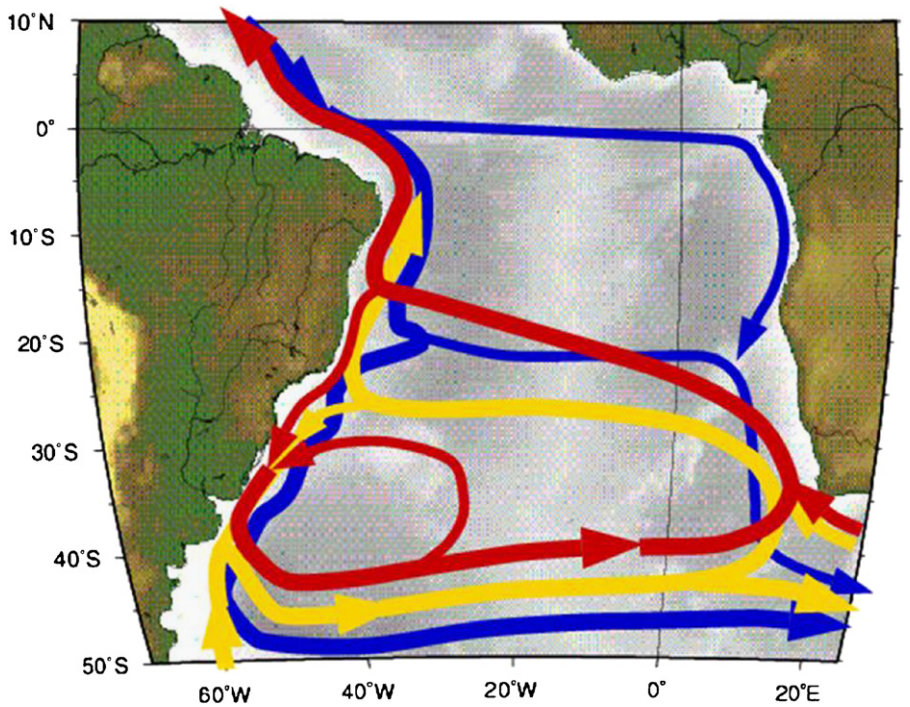

Fig. 1. A schematic representation of the large-scale circulation of North Atlantic Deep Water (NADW) (blue), Antarctic Intermediate Water (AAIW) (yellow), and South Atlantic Central Water (SACW) (red). Adapted from the results of Stramma and England (1999).

encounter takes place at approximately 38°S and creates a strong thermohaline front with temperature gradients as high as 1 °C/100 m that has been named the Confluence or Confluence Front (Gordon and Greengrove, 1986). The poleward (southward) transport of the Brazil Current varies with latitude, reaching values as high as 30 Sv, most of which is typically confined to the upper 1000 m (Garzoli, 1993; Ganachaud and Wunsch, 2003). The Malvinas Current, a branch of the Circumpolar Current, is the main conduit of Pacific water into the subtropical South Atlantic. This current flows north along the eastern edge of the continental shelf of Argentina to latitudes as far north as 38°S (Piola and Gordon, 1989; Garzoli, 1993). The Malvinas Current is mostly uniform with depth, and estimates of the volume transport obtained from hydrographic data using a level no motion at the bottom of the AAIW vary between 10 and 15 Sv (Gordon and Greengrove, 1986; Garzoli, 1993). However, mass conservation in the region points toward the presence of significant bottom velocities along the continental slope near the Brazil–Malvinas Confluence (Peterson, 1992; Vivier et al., 2001).

A marked variability in the location of the Confluence Front along the coast of up to 900 km has been observed both from surface observations (Olson et al., 1988) and subsurface observations (Garzoli and Bianchi, 1987; Garzoli and Garraffo, 1989). During the austral summer (January–March), the Brazil Current reaches its southernmost extension while the Malvinas Current retreats (e.g. Garzoli et al., 1992). An opposite situation is observed during the austral winter (June–August), when Malvinas waters reach their northernmost latitudes. Significant interannual variability has also been observed (Olson et al., 1988; Garzoli, 1993). The variability of the Confluence Front is due to the seasonal cycle of the wind stress curl in the subtropical South Atlantic (Matano et al., 1993), and the interannual variability is forced by anomalous wind patterns south of the confluence region (Garzoli and Giulivi, 1994).

The South Atlantic thermocline and sub-Antarctic inflow are derived from the eastward-flowing South Atlantic Current (Stramma and Peterson, 1990), part of which turns northward into the Benguela Current (Fig. 1). The Benguela Current is the broad northward flow adjacent to southwestern Africa that forms the eastern limb of the South Atlantic subtropical gyre, and is the origin of the upper layer water that flows northward across the equator into the North Atlantic. The Indian Ocean water is injected into the Benguela Current through Agulhas eddy shedding and Agulhas Retroflection filament processes (Lutjeharms and van Ballegooyen, 1988; Shannon et al., 1989). Observations reveal that at 30°S the Benguela Current transport consists of a nearly steady flow confined between the southern African coast and approximately 4°E (amounting to 10 Sv in the mean), and a more variable flow (3 Sv in the mean) between 4°E and the Walvis Ridge (Garzoli and Gordon, 1996). From trans-basin sections, estimates of the northward transport east of the Mid-Atlantic Ridge have varied from 16 Sv (Ganachaud and Wunsch, 2003) to 23 ± 10 Sv (Macdonald, 1998). It has also been observed that a minimum of four to six rings originating from the Agulhas retroflection enter the South Atlantic each year, and that the eddy field is responsible for an average transport of 0.02 PW between the Atlantic and Indian Oceans (Duncombe Rae et al., 1996; Goñi et al., 1997; Garzoli et al., 1999).

Donners and Drijfhout (2004) analyzed the product of a global ocean general circulation model (OCCAM) to investigate the inter-ocean exchange of thermocline and intermediate waters in the South Atlantic using a Lagrangian path-following technique. Results of the analysis suggest that most (>90%) of the South Atlantic flow towards the north originates from the Indian Ocean via leakage from the Agulhas Current system. Agulhas leakage into the South Atlantic occurs from the surface to depths as great as 2000 m. This relatively warm water (temperatures higher than 10 °C on average) leads to relatively large meridional heat fluxes in the band 30°–35°S. From the same OCCAM product, de Ruijter et al. (2004) calculated the time variable heat flux at 30°S and found that the mean annual value for the heat transport is 0.58 PW, with an annual cycle ranging from 0.5 to 1.1 PW ($\mathrm{PW} = 10^{15}$ W).

Numerous studies have been conducted to calculate the heat transport in the global ocean using different methods. These include direct observations (e.g., Talley, 2003), inverse models (e.g. Lumpkin and Speer, 2007; Ganachaud and Wunsch, 2003; Macdonald et al., 2001; Rintoul, 1991; Fu, 1981), numerical models (e.g. Matano and Philander, 1993; Saunders and Thompson, 1993; Saunders and King, 1995) and residual methods (e.g. Trenberth and Solomon, 1994). Within the subtropical region, in the 30°–33°S band, the heat

flux estimates range from small southward values (e.g., −0.23 PW, de las Heras and Schlitzer, 1999) to close to 1 PW northward (0.94 PW, direct method, Saunders and King, 1995; 0.88 PW, inverse model Fu, 1981). In a recent paper Lumpkin and Speer (2007), using a combination of direct and residual methods, obtained a value of 0.60 ± 0.08 PW across the A11 WOCE line (nominally 40°S). This value is in the range of values obtained by Saunders and King (1995) from direct observation along A11 (0.45–0.94 PW; preferred value 0.88 PW). Large heat transport variability may be a real feature of the South Atlantic circulation due in part to the large variability of the boundary currents. Both margins are characterized as highly energetic and variable regions. However, given the widely varying estimates more work is needed to understand and resolve the variability.

In 2002, as part of the NOAA Global Ocean Observing System, a new expendable bathythermograph (XBT) high-density line (AX18) was started in the South Atlantic between Cape Town, South Africa, and Buenos Aires, Argentina. Before 2004 this line was sampled twice a year. Since 2004 four occupations per year have been conducted. The line was designed to monitor the upper layer mass budget in the South Atlantic and to estimate the variability of the upper limb of the MOC transport. This paper presents results from 14 transects that have been occupied (Fig. 2, Table 1). In this paper, new estimates of the meridional heat transport obtained from the data collected along AX18 are presented and the results discussed in terms of the South Atlantic variability.

2. Data and methodology

Given observed values of the temperature (T), salinity (S) and meridional velocity (v) fields the meridional volume (V) mass (M) and heat (H) transport are defined as

$$V = \int\int v\,dx\,dz \quad [Sv = 10^6\,m^3/s],$$

$$M = \int\int \rho v\,dx\,dz \quad [kg/s],$$

$$H = \int\int \rho c_p T v\,dx dz \quad [PW = 10^{15}\,W],$$

where ρ is the density of the water and c_p the specific heat capacity.

The total meridional velocity (v) can be decomposed into 3 components:

$$v = v_g + v_{ag} + v_b,$$

v_g is the geostrophic (baroclinic) component, which can be estimated from the hydrographic field, v_b is the barotropic component (here defined as the reference velocity used to make v_g absolute), and v_{ag} is the ageostrophic component, which is assumed to be wind-forced Ekman transport. Meridional Ekman transports are computed as the Ekman mass, M_y, and Ekman heat, H_y, transport given by

$$M_y = -\frac{\tau_x}{f}\Delta x,$$

$$H_y = M_y c_p T_{EK},$$

where τ_x is the zonal component of the wind stress, f is the Coriolis parameter, Δx is the horizontal

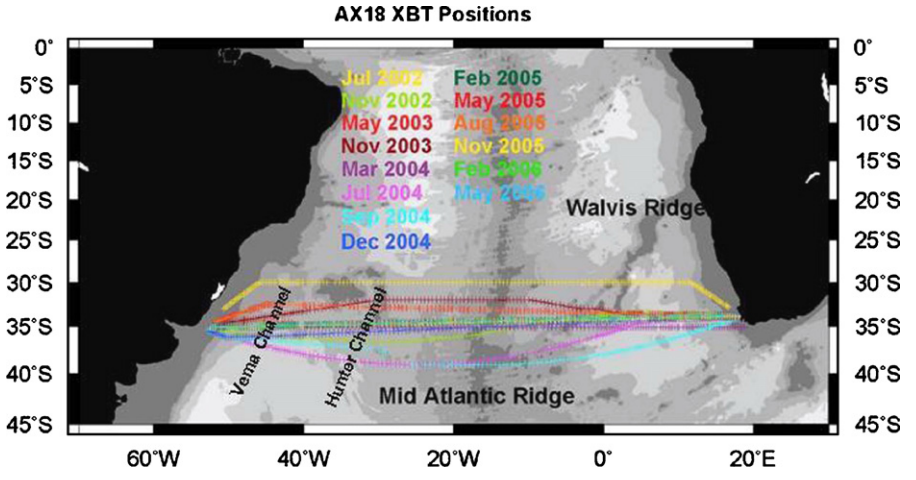

Fig. 2. Location of the 14 transects conducted along the XBT high-density line AX18.

Table 1
Detailed specification of average positions of each XBT section

Month	Western Lon	Western Lat	XBT depth (m)	Eastern Lon	Eastern Lat	XBT depth (m)	Mean Lat
Jul-02	50° 38′W	32° 59′S	101.2	16° 40′E	32° 49′S	859.8	30° 19′S
Nov-02	52° 20′W	35° 16′S	814.4	17° 29′E	33° 40′S	423.5	35° 03′S
May-03	52° 23′W	34° 59′S	153.4	17° 53′E	33° 52′S	208.5	34° 22′S
Nov-03	52° 06′W	34° 45′S	195.4	17° 50′E	33° 40′S	196.7	33° 13′S
Mar-04	52° 36′W	35° 04′S	128.3	18° 49′E	35° 04′S	219.0	35° 04′S
Jul-04	52° 35′W	35° 26′S	200.0	14° 08′E	34° 00′S	819.6	36° 42′S
Sep-04	52° 48′W	35° 25′S	117.7	17° 56′E	33° 58′S	202.0	37° 09′S
Dec-04	52° 44′W	35° 26′S	149.4	18° 00′E	33° 52′S	173.1	35° 02′S
Feb-05	52° 20′W	35° 03′S	159.9	17° 52′E	33° 52′S	213.8	34° 27′S
May-05	51° 51′W	34° 25′S	153.4	17° 48′E	33° 51′S	254.3	33° 41′S
Aug-05	51° 51′W	34° 28′S	166.5	18° 04′E	33° 52′S	143.5	33° 17′S
Nov-05	52° 29′W	35° 05′S	150.1	17° 53′E	33° 52′S	204.7	34° 27′S
Feb-06	52° 22′W	35° 01′S	147.5	17° 44′E	33° 40′S	215.8	34° 20′S
May-06	52° 23′W	35° 01′S	144.2	17° 45′E	33° 40′S	208.6	34° 20′S

"XBT dpth" indicates the maximum depth to which good temperature data was collected from the XBT. All XBTs listed except the easternmost XBTs during July 2002 and July 2004 hit the bottom and fully sampled the water column. Mean latitude is the mean latitude of each transect.

distance and T_{EK} is the mean temperature of the Ekman layer. Ekman transports are determined using NCEP daily reanalysis winds. The NCEP reanalysis winds were provided by NOAA-CIRS Climate Diagnostic Center, via their web site at http://www.cdc.noaa.gov.

Ekman heat flux in PW, H_y, is calculated from:

$$H_y = M_y c_p (T_{EK} - T_{section}),$$

where M_y is the Ekman mass transport. The Ekman layer temperature, T_{EK}, is computed from deep climatological values obtained from the High Resolution (0.25°) Temperature and Salinity Climatology produced by Boyer et al. (2006) (WOAO.25), with the mixed layer depth defined as extending from the surface to a depth where ΔT is 0.1 °C from the surface value. $T_{section}$ is the spatial average of the WOA0.25 annual mean section.

The methodology used to obtain the baroclinic component of the heat transport from the XBT data collected along AX18 is thoroughly described and tested in Baringer and Garzoli (2007). In short, salinity (S) is estimated for each XBT profile by using S (T, P, latitude, longitude) derived from ARGO and CTD data following the methodology described by Thacker (2007). Full-depth temperature/salinity profiles are obtained by extending the profiles to the bottom of the ocean using WOA0.25 below the depth measured by XBTs (typically 850 m). The method was tested using the WOCE A10 line along 30°S by successively degrading the CTD observations until they finally appear as if the original data were nothing more than 850 m XBTs.

Geostrophic velocities are determined using the dynamic method where a level of no motion was chosen at $\sigma_2 = 37.09\,kg/m^3$ (σ_2 defined as potential density relative to 2000 dbar). This deep reference level produces transports comparable with previous observations and was chosen following previous heat transport estimates (Ganachaud, 2003). For instance, the flow of Antarctic Bottom Water (AABW) has been estimated at 4 ± 0.4 Sv in the Vema Channel (Hogg et al., 1982) and 2.9 ± 1 Sv in the Hunter Channel (Zenk et al., 1999) for a total of about 7 Sv across 30°S (see Fig. 2 for locations). As the flow moves northward, the transport of AABW decreases (e.g. 5.5 ± 2 Sv at 11°S, McCartney and Curry, 1993). Since most of the AX18 sections are south of 30°S where we expect the transport of AABW to be higher still, we require that the net northward transport of AABW west of the Mid-Atlantic Ridge fall in a slightly higher range between 5 and 11 Sv. Ganachaud and Wunsch (2003) noted that, because of the Walvis Ridge and the adjacent topography, any section crossing the ridge is closed below 4000 m for northward flow east of the ridge and for southward flow between the Walvis and Mid-Atlantic Ridge (Fig. 2). Accordingly, the net transport below 4000 m should be minimal (0 ± 2 Sv). In addition this deep reference level reproduces transports at the boundaries that

Table 2
Transport estimates for each of the XBT transects where "Date" is the date when the cruise was started, "Ekman" is the Ekman heat flux, "Geostrophic" is the geostrophic component of the heat transport, and "Total HT" is the final value obtained for the heat transport

Heat transport (PW)				Volume transport (Sv)	
Date	Ekman	Geostrophic	Total	East of 3°E (0–800 m) Sv	Brazil Current (0–800 m) Sv
Jul-02	0.16	0.25	0.4	17	−25
Nov-02	0.08	0.4	0.48	24	−25
May-03	0.21	0.32	0.54	24	−21
Nov-03	0.07	0.42	0.49	30	−22
Mar-04	0.01	0.60	0.60	21	−12
Jul-04	0.24	0.27	0.50	21	−12
Sep-04	0.16	0.51	0.68	20	−17
Dec-04	0.02	0.79	0.81	21	−24
Feb-05	0.01	0.47	0.48	26	−12
May-05	0.04	0.52	0.56	30	−15
Aug-05	0.15	0.27	0.42	27	−20
Nov-05	−0.01	0.48	0.47	21	−18
Feb-06	−0.02	0.61	0.59	22	−20
May-06	0.13	0.37	0.49	24	−20

Units are PW ($1\,PW = 10^{15}\,W$) and Sv ($1\,Sv = 10^{6}\,m^3/s$).

are in agreement with previous observations (see discussion of Table 2).

The analysis of a general circulation model allowed Baringer and Garzoli (2007) to determine that the initial velocity field is adjusted along the western boundary because of the barotropic flow arising from the Brazil Current and North Atlantic Deep Water flowing in the same direction (Fig. 1). Current meter measurements at 35°S confirm southward bottom velocities on the order of 0.04 to 0.06 m/s (Flood and Shore, 1988). Peterson's (1992) review of bottom velocity observations in the region of the Brazil Malvinas confluence quoted an average of $v = -0.04$ m/s. Based on these observations, the AX18 velocity field is adjusted by this value over an areal extent so that the resultant value of the deep current is between 5 and 10 Sv. After the bottom velocity correction is applied, the net transports are evaluated and a uniform velocity correction is applied to guarantee that the total salt flux across each section matches the salt flux through the Bering Straits (27.6×10^6 kg/s, Coachman and Aagaard, 1988). This velocity is uniformly applied across the entire section and values are quite small (10^{-4}–10^{-6} m/s).

The heat transport estimates contained herein are subject to uncertainties that include issues specific to XBT observations and those inherent in any heat transport calculation based on hydrographic data (see Part I for a complete discussion). The total uncertainty is thus estimated to be ±0.18 PW.

3. Results: heat transport from the AX18 data

In this section the analysis of the heat transport across AX18 is presented (Fig. 3). Estimates of the total heat transport and the geostrophic and Ekman contributions as obtained in this paper are listed in Table 2 together with the integrated volume transport for the southward flowing Brazil Current and the northward flow east of the Walvis ridge (~3°E at 35°S). The latter is an indication of the northward flowing Bengula Current. Volume estimates are provided from the surface to 800 m, the depth covered by the XBT observations. The mean value of the volume flow east of 3°E is 23 Sv with a standard deviation of ±4 Sv. These values are in agreement with those previously obtained for the Benguela Current by Garzoli and Gordon (1996), 16 Sv; Ganachaud and Wunsch (2003), 16 Sv; Macdonald (1998), 23 Sv; Fu (1981), 20 Sv; Shannon (1985), 15 Sv; and Stramma and Peterson (1989) 21 Sv at 32°S and 18 Sv at 30°S. The mean value for the southward flow associated with the Brazil Current is 19 Sv with a standard deviation of ±4 Sv. The weak Brazil Current flow intensifies by about 5% per 100 km as it flows south of 24°S (Peterson and Stramma, 1991). At about 33°S the total transport (which includes a recirculation cell in

the upper 1400 m) is about 18 Sv, and reaches values from 19 to 22 Sv at about 38°S, where the Brazil Current encounters the Malvinas Current (Olson et al., 1988; Peterson and Stramma, 1991).

The Ekman heat transport is shown in Fig. 4 as a function of time and latitude. Averaged mixed layer properties used to calculate the heat transport are obtained from the WOA0.25 climatology; results are very similar when XBT-derived values are used. Generally Ekman heat transports decrease towards the equator. The zero contour line migrates meridionally between 28° and 34°S following an annual and semiannual signal. The maximum positive value of the Ekman heat flux is, on average, 0.3 PW, observed during June-August at 38°S. Interannual variability can be as much as 0.3 PW (e.g. along 36°S, Fig. 4). In addition to natural variability of the fluxes at a fixed latitude, there is a possible ambiguity in interpreting the time variability of the XBT-derived heat transport estimates because each vessel deploying XBTs may follow different routes across the ocean basin, hence sampling different latitudes within a strongly varying wind field. This uncertainty could be as much as 0.4 PW if, for example, comparisons were made between heat transport estimates in March at 32°S and 36°S. However, Fig. 4 shows that merchant ships tend to favor benign weather and follow latitudes where the winds are generally weaker (and easterly). Thus, transects occurred mostly during times when Ekman heat transport varied from 0 to 0.2 PW (see also Table 2). Ekman fluxes were also calculated from Hellerman and Rosenstein (1983) winds, NCEP daily winds, NCEP monthly climatological winds and from satellite winds (not shown). Results indicated that the use of different wind products caused the values obtained for the mean heat transport across 35°S to vary by less than ± 0.04 PW; thus all wind products produce reasonable mean values. The largest variability, and hence uncertainty, for individual heat transport values reflects both space and time differences. Essentially,

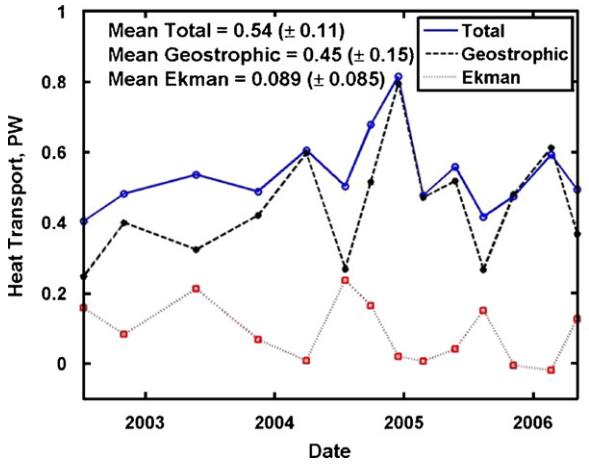

Fig. 3. Heat transport from data collected during the different cruises. Solid blue line: total heat transport; Dashed black line: geostrophic component; Dashed red line: Ekman component. All values are in PW (1 PW = 10^{15} W).

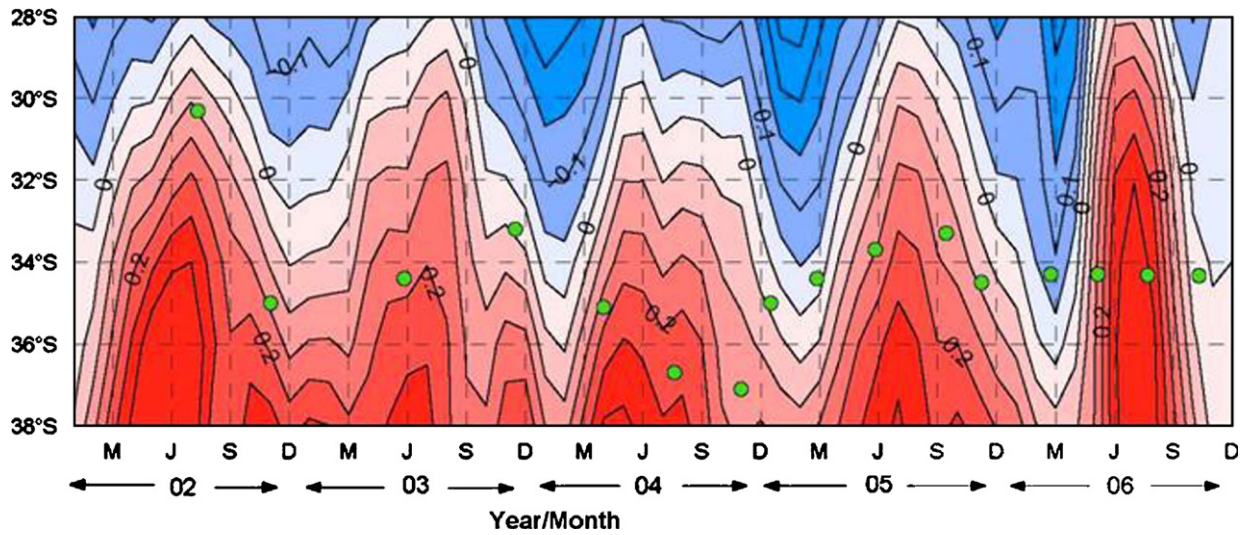

Fig. 4. Ekman heat flux, H_y, in PW as a function of time and latitude calculated from the NCEP monthly winds. Each XBT section is noted (green dot) by the mean time and latitude the section occurred. Note that the XBT transects appear to follow fairly benign weather, and that natural variability in Ekman transports may be larger than that observed on the sections themselves.

any individual estimate may be relatively well constrained (e.g. ± 0.04 PW, Baringer and Garzoli, 2007); however, additional uncertainty can arise from ascribing changes in heat transport values to temporal variability without consideration of the spatial variability.

The analysis of the geostrophic heat transport is straightforward, as outlined previously; however, three of the fourteen XBT sections did not completely cross the entire Atlantic basin because of weather, equipment malfunctions, etc. Typically, hydrographic sections are considered to be complete according to WOCE specifications if observations are collected up to and including the 200 m isobath, and the majority of the sections presented herein meet this criteria. Table 1 lists the westernmost and easternmost stations and the beginning/ending XBT depths for all the sections taken to date (note that most of the failures occurred at the beginning of the program). In particular, sections in July 2002, Nov 2002 and July 2004 were commenced late or terminated early. These sections failed to sample the complete transect, and hence estimates of the missing transports are needed. In what follows are detailed discussions of two example sections where the whole basin was sampled (March 2004 and May

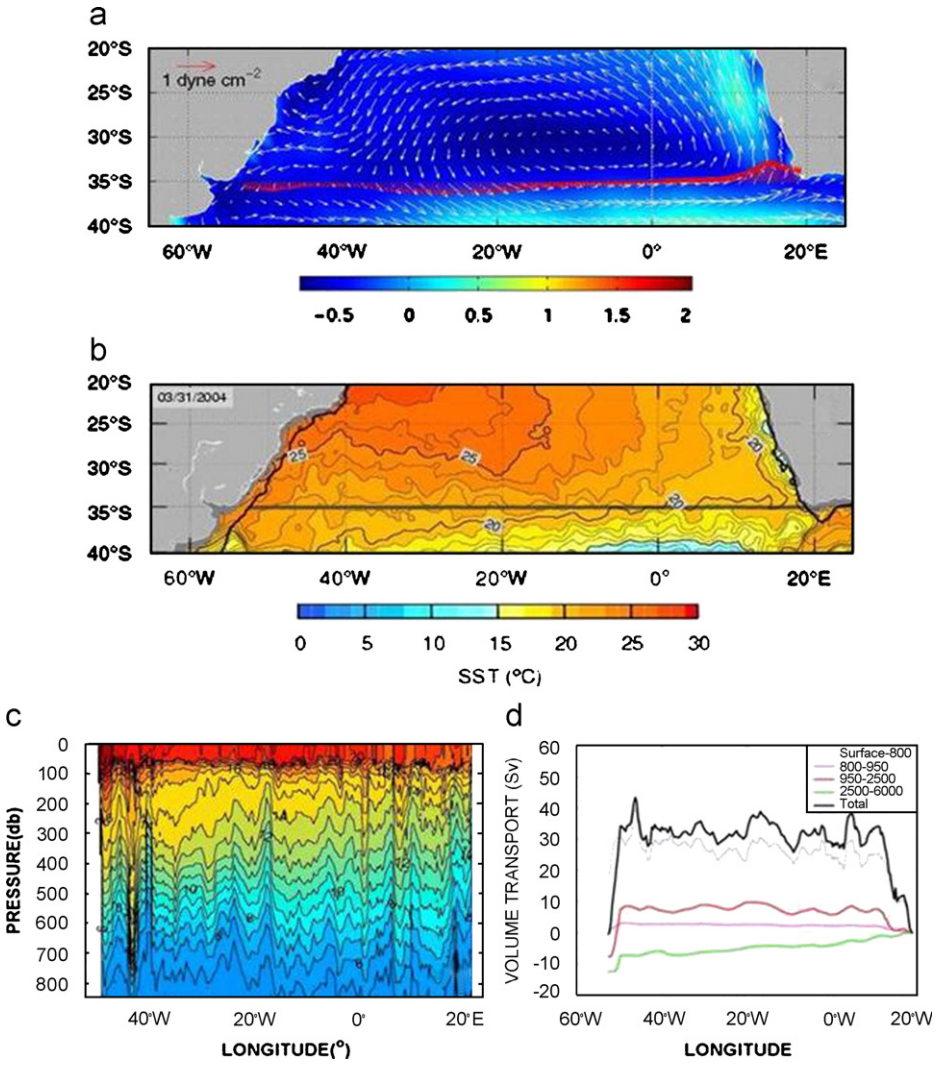

Fig. 5. (a) NCEP wind stress in dyne cm^{-2} for the region during the March 2004 section. The wind stress was interpolated to the XBT location and date from the monthly NCEP data (solid red arrows). (b) Sea surface temperature (SST) is shown averaged during the time of the cruise in °C with the cruise track-line shown black. (c) The March 2004 vertical temperature section is shown in °C. (d) The cumulative (starting from the eastern end of the section) volume transport is computed for different depth ranges.

2006), and sections that required transport corrections in the western (November 2002) and eastern (July 2004) boundaries.

3.1. March 2004

This cruise was conducted along 35°S. The cruise track is shown in Fig. 5 plotted with the wind field (Fig. 5a) and the SST field (Fig. 5b); temperature data collected with the XBT are shown as a function of depth in Fig. 5c next to the cumulative volume transport estimates (Fig. 5d) using the methodology described before. The plotted wind field was obtained from the NCEP reanalysis and is an average during the cruise (days 76–107, 2004). The wind stress forms a large anticyclonic gyre centered on 10°W with southward wind stress parallel to the South American coastline and northward along the African coast. The resultant Ekman heat transport integrated across the basin is low (0.01 PW, Table 2). According to previous observations (Garzoli and Garraffo, 1989; Goñi and Wainer, 2001), at this time of the year the Malvinas Current should have been retracted from its northernmost extension and should no longer be present in the area. The SST satellite image (Fig. 5b) shows that this is indeed the case. The Brazil Current is at its southernmost extension, south of 37° 30′S. At the

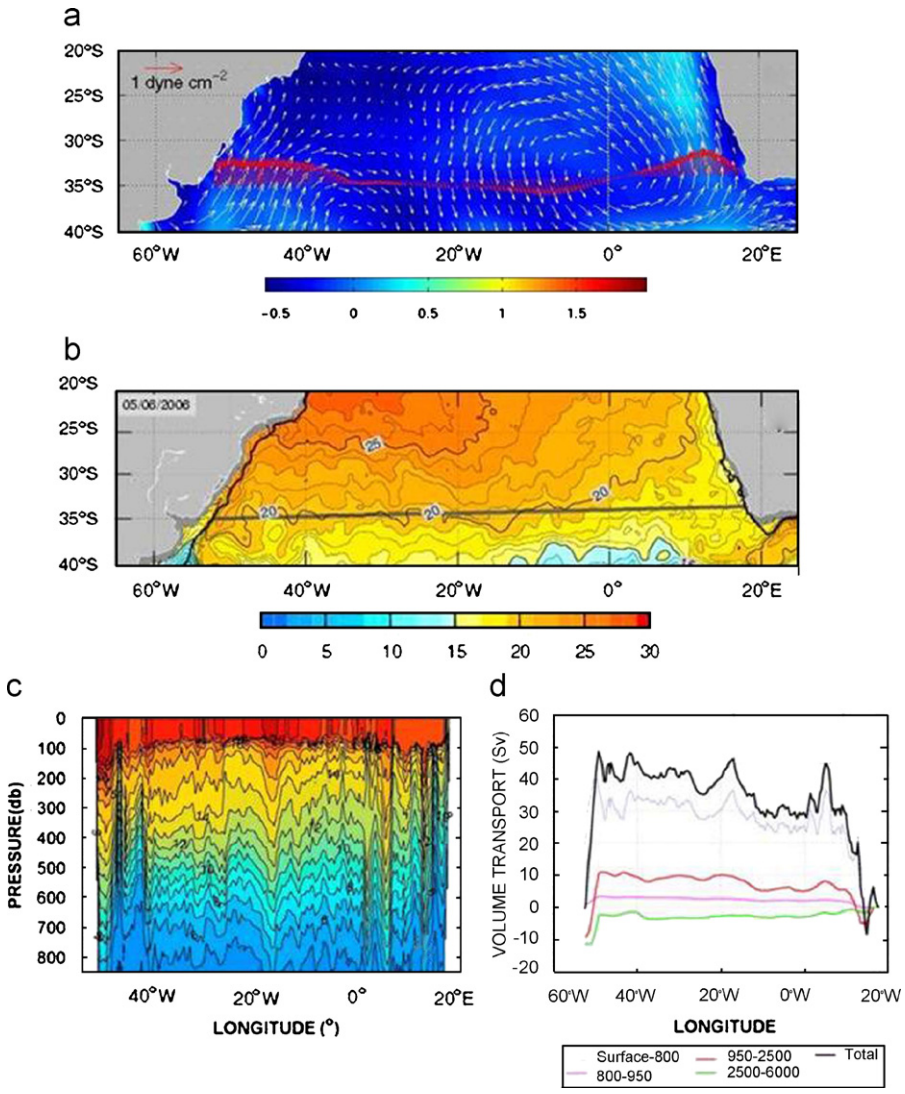

Fig. 6. (a) Wind stress, (b) SST, (c) vertical temperature section, and (d) cumulative volume transport (as in Fig. 7) for March 2006 section.

western boundary the vertical section of temperature shows the southward flowing Brazil Current west of 40°W, and a warm Brazil ring centered at 46°W (Fig. 5d). Agulhas rings are observed at 3°W and 4°E and a broad Benguela Current is observed flowing northward east of 8°E. The fact that the temperature structures described above are associated with rings is confirmed from analysis of the sea surface height fields (not shown). All these features are also shown in the integrated volume transport (Fig. 5d). The Brazil Current in the upper 800 m has a total volume transport of 12 Sv and the DWBC (2500–6000 m) −6 Sv. In the center of the basin, between the Walvis Ridge (0′E) and 40 °W, the net transport is very close to zero (2 Sv). The easternmost XBT station hit the bottom at 219 m, and the westernmost XBT reached 128 m depth (i.e. on the shelf, Table 1). Therefore, the section completely sampled the ocean basin (except for shelf transport which is accounted for in the error bars) and hence there is no need to make major corrections for missing flow at the boundaries. We conclude that the total heat transport across the March 2004 section is 0.60 PW, with an uncertainty of ±0.18 PW.

3.2. May 2006

A different situation was observed during May 2006. The cruise was conducted at a similar latitude as during March 2004 (mean latitude = 34°20′S, Table 1). The cruise track is shown in Fig. 6 which also shows the wind stress during the time of the cruise (Fig. 6a), the sea surface temperature (Fig. 6b) and the vertical section of temperature as observed with the XBT data and the integrated

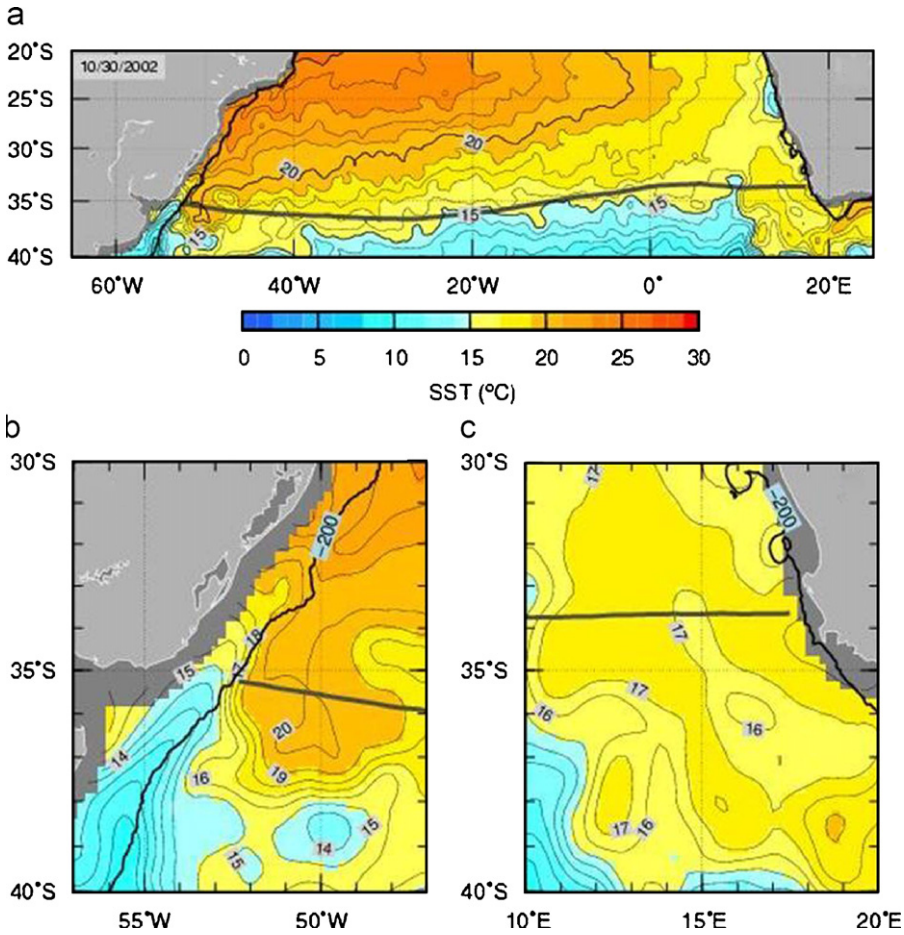

Fig. 7. (a) Average SST in °C for the duration of the cruise (top panel) conducted during November 2002. The solid line indicates the ship track. Lower panels are close up figures detailing the SST in °C at the (b) western and (c) eastern boundaries. All contours are in °C with intervals of 1 °C (solid lack lines).

transport across the basin (Fig. 6c and d). At this time of year, the anticyclonic circulation in the wind stress is centered at 0°E while a cyclone is located off the coast of Argentina. As a result, the integrated Ekman flux is larger than during the March 2004 section (0.13 PW, Table 2), and the net volume transport in the center of the basin (0°E–40°W) is larger, 15 Sv. However, the total integrated heat transport is lower (0.49 PW, Table 2) because the geostrophic component of the heat flux is much lower (0.37 PW, Table 2). The integrated transport (Fig. 5d) panel shows that a southward flow is observed at the eastern boundary consistent with the observations collected by Richardson and Garzoli (2003), a stronger DWBC is observed at the western boundary (−9 Sv), and the Brazil Current has a southward flow of −20 Sv. All of these features contributed to a smaller northward geostrophic component of the flow. Also it must be noted that west of 20°W the SSTs are higher (Fig. 6) than those observed during March 2004 (Fig. 5). The Malvinas Current has begun its northward migration and the SST picture shows cold temperatures associated with the current as far north as 37°S flowing over the Argentine continental shelf. The vertical distribution of temperature (Fig. 6c) shows a confined Brazil Current in the western boundary and a wider Benguela Current in the east. The temperature structure observed at 5°E is associated with an Agulhas retroflection ring. Data was collected along the whole section with the westernmost station at 144 m depth and the easternmost station at 209 m. The total heat transport obtained is 0.49 PW with an uncertainty of ±0.18 PW.

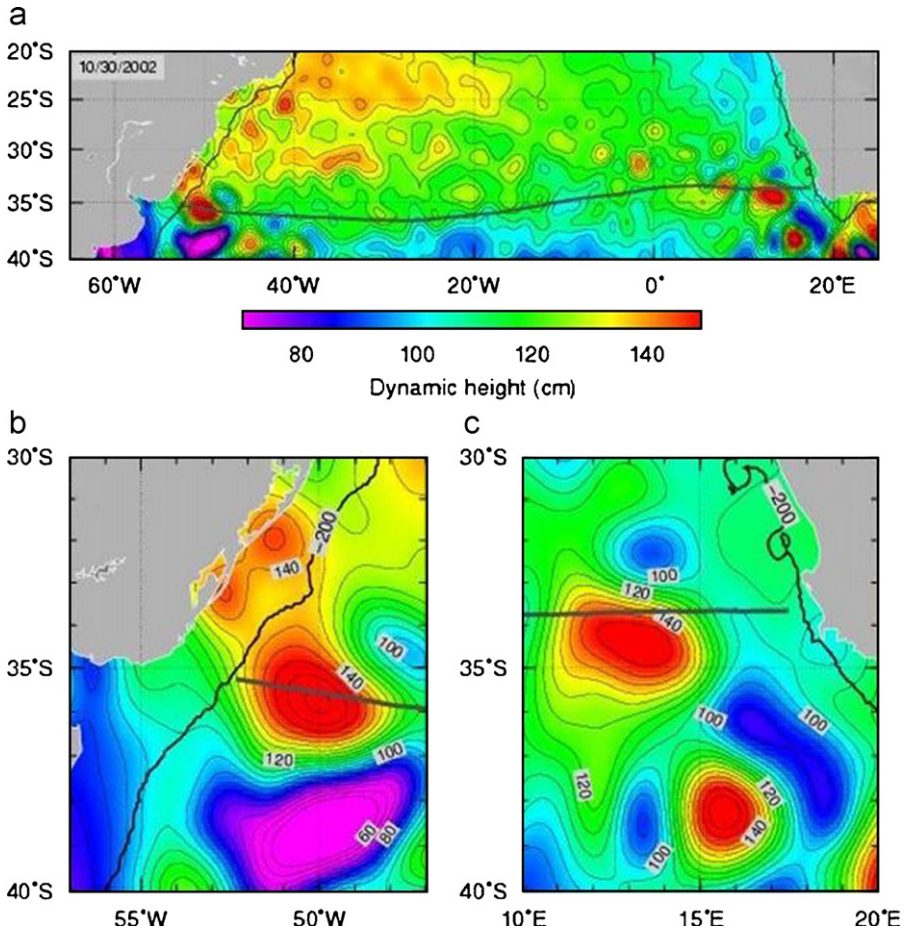

Fig. 8. (a) Sea surface height derived from altimeter anomalies for November 2002 (courtesy of G. Goni). The top panel shows the dynamic height in centimeters during the cruise (track shown as solid white line) and the lower panels are the details at the (b) western and (c) eastern boundaries. All panels use contours of 5 dynamic centimeters (solid black lines).

3.3. November 2002

This line was conducted along approximately 35°S latitude (Fig. 7) from October 29 to November 6, 2002. According to observational studies (e.g. Olson et al., 1988; Garzoli and Garraffo, 1989), the Malvinas Current should be receding from its northernmost extension during this time of year. The SST satellite image (Fig. 7) shows that the there is a strong SST front near 36°S, i.e. its location is slightly to the north of the expected mean position of the Malvinas Current for that month. Most of this flow is on the shelf and contains a mixture of water from the relatively cold and fresh southern shelf water, the Rio de la Plata (La Plata River) outflow and the southward flowing Brazil Current.

The estimated heat transport across the section where data are available (up to 52°20′W) is 0.49 PW. The westernmost XBT station was collected in 814.4 m of water (i.e., on the continental slope). Therefore, it failed to sample a portion of the shelf water and its return flow along the continental shelf, as well as portion of the Brazil Current along the continental shelf slope which is typically positioned between the 200 and 830 m isobaths. The SST map (Fig. 7c) indicates that there is a Brazil Current Ring centered at approximately 36°S49°W that is ready to detach from the main Brazil Current. This is confirmed by the sea surface height derived from altimeter data (Fig. 8). The missing transport can be estimated from the dynamic height field shown in Fig. 8. Assuming that the ring is symmetric, the result is a small flow of 0.18 Sv. A correction to the heat transport due to this ring can be estimated as

$$\Delta HT = \Delta V(T_m - T)c_p\rho_0,$$

where ΔV is the missed volume transport, T_m is the mean temperature of the section, T is the temperature of the flow, c_p is the specific heat and ρ_0, the density of water. This small transport correction

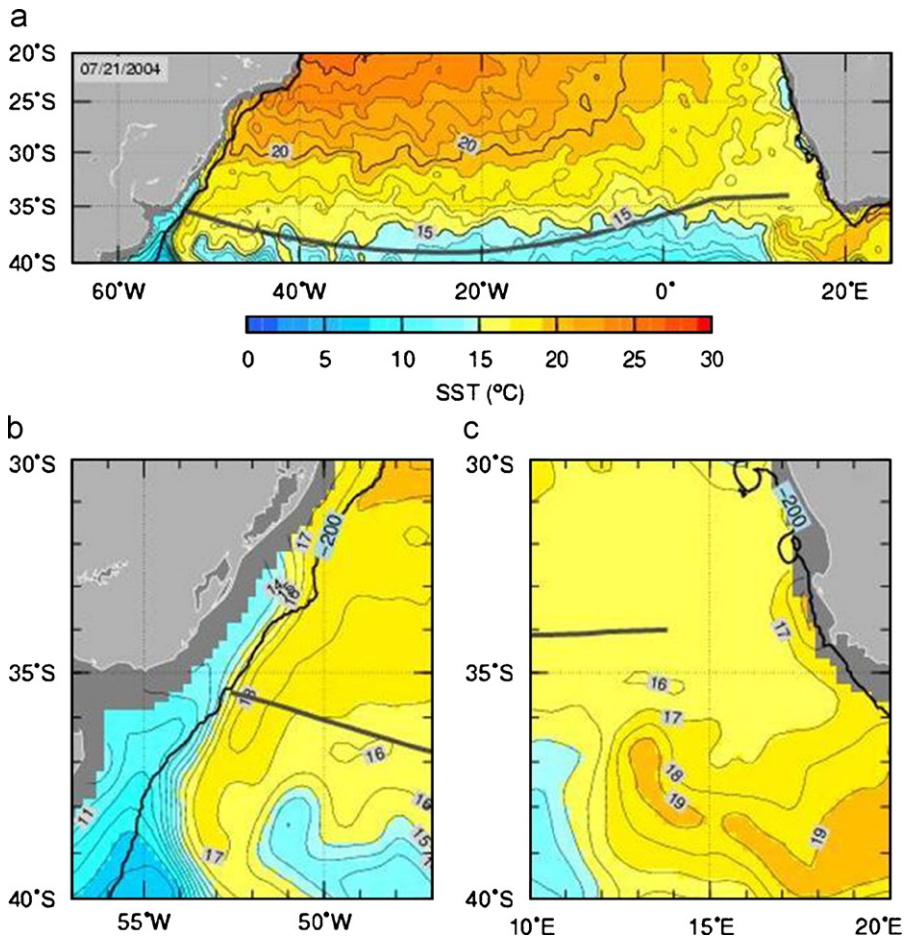

Fig. 9. Average SST (as in Fig. 9) for the July 2004 cruise.

leads to a change in the heat transport of −0.01 PW. If the amount of missing flow (0.18 Sv) is 100% uncertain (±0.18 Sv), this will lead to an additional uncertainty of ±0.01 and the estimated heat transport becomes 0.48±0.18 PW (Table 2).

3.4. July 2004

This line was conducted approximately along 37°S and is one of the southernmost section occupied to date (Fig. 2, Table 1). During the month of July according to previous observations (e.g., Garzoli and Garraffo, 1989; Goñi and Wainer, 2001), the Malvinas Current should be at its northernmost extension. The SST satellite image (Fig. 9) shows the presence of the cold shelf water as far north as almost 31°S. As in the November 2002 section, it is confined to the shallow waters of the continental shelf (water depths <200 m) and hence is likely a mixture of river outflow and cold/fresh southern shelf water. The westernmost station was occupied near the 200-m isobath, and, therefore, the section was completely sampled on this side of the ocean. However, because of malfunctioning equipment, the easternmost XBT stations were lost and the first good XBT was collected at 14°08′E. Hence, there is a need to account for the flow typically found between 14°08′E and the eastern boundary that was not sampled. The sea surface height map of the region (Fig. 10c) indicates the presence of an Agulhas ring centered at approximately 33°30′S 14°30′E, just east of where the first good XBT was deployed. The flow in this area was estimated in two different ways: use of altimetry and use of WOA0.25 data. The values of dynamic height obtained with the altimeter data indicate a transport of about 3 Sv. This missing volume transport leads to an increase in the heat transport of 0.15 PW. Alternatively, using the full water column WOA0.25 climatological data to complete the section to the

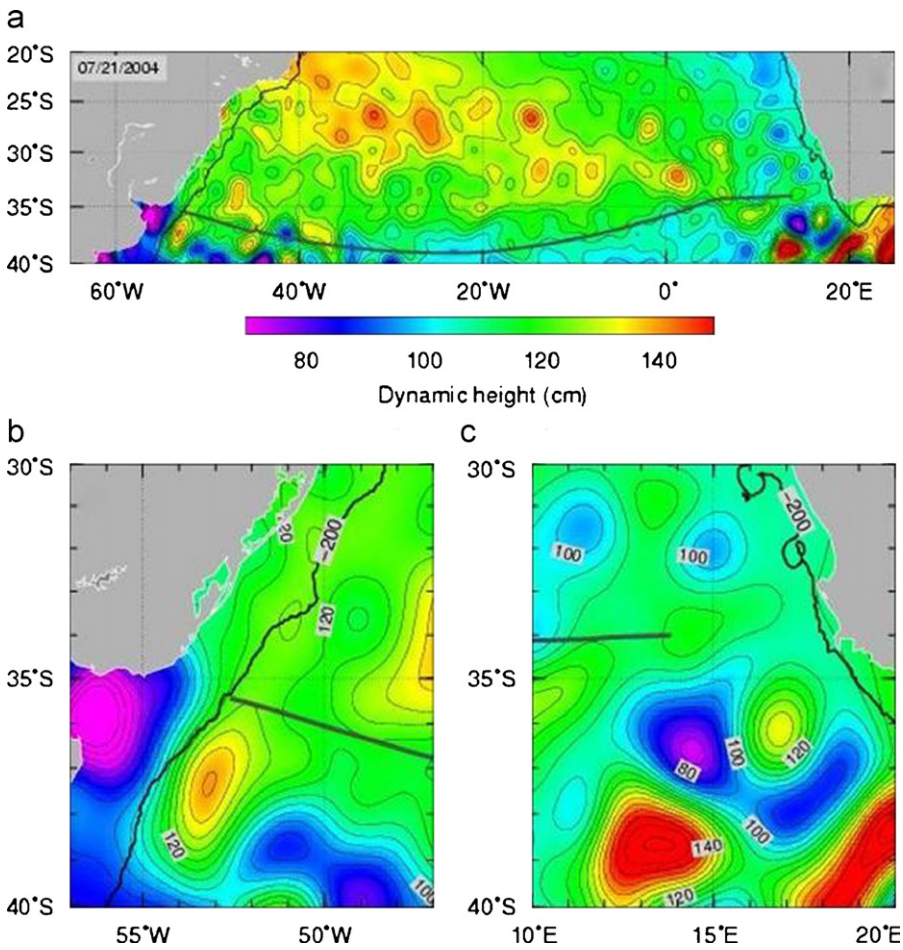

Fig. 10. Sea surface height for the July 2004 cruise (as in Fig. 10).

boundary, also leads to an increase in the heat transport of 0.15 PW. Without any correction for the missed flow at the boundaries, the heat transport estimate for the section was 0.35 PW. Adding this correction, the estimated net heat transport becomes 0.50 PW (Table 2). Note that the section conducted during July 2002 (not shown) was adjusted in the same manner as the July 2004 section. The July 2002 section was also the only section conducted along 30°S (see Table 1). This location is similar to the one occupied during the WOCE 30°S CTD section (A10). Perhaps fortuitously, the value of the meridional heat transport obtained in the present paper is similar (0.40 PW) to the one obtained by Ganachaud (2003) for A10 (0.40 PW).

5. Discussion and conclusions

Fourteen high-density XBT sections were used to infer the meridional heat transport in the South Atlantic. The integrated volume transport obtained from the methodology applied yields a mean value for the total transport east of the Walvis ridge of 23 Sv, balanced by 19 Sv of Southward flowing Brazil Current (between 0 and 800 m), (Table 1), and 9 Sv of Southward DWBC (2500–6000) (not shown). The net flow in the center of the basin ranges between 0 and 30 Sv depending on the wind structure (not shown). The values obtained in this paper for the heat transport (Table 2 and Fig. 3), ranged from 0.40 to 0.81 PW with a mean value of 0.54 PW and a standard deviation of 0.11 PW. Fig. 3 displays the variability of the different components of heat transport during the time of the observations. The total heat transport shows a pronounced increase from July 2004 to December 2004 and a decrease thereafter. It also indicates some variability that may be natural variability or may be related to the difference in cruise track. In order to determine if the latter is the case, we analyze the variability of the transports as a function of the mean latitude (Fig. 11). It is known (Fig. 4) that the Ekman flux has a pronounced annual cycle that varies with latitude. To illustrate the effect of eliminating the variability with latitude associated with the Ekman heat transport, both the total heat and the geostrophic transport are shown in Fig. 11. There is no obvious relationship between the geostrophic transport (what is actually measured) and the latitude. For the latitude band 33°–36°S, transports vary between 0.28 and 0.81 ± 0.08 PW. Fig. 11 demonstrates that there is little convincing evidence that changes in the cruise track are a dominant source of variability for geostrophic heat transport, but there is a slight suggestion that southern latitudes may have a bias of as much as 0.14 PW per 3° of latitude for the total heat transport, consistent with the changes in Ekman transport. Most importantly, the maximum heat transport is observed in December 2004 along a line that was conducted at approximately 35°S, only slightly further south than the mean latitude of all the sections (approximately 33°20′S). Therefore, the long-term interannual variability (on the order of 0.4 PW peak to peak) is not convincingly driven by aliasing of the sections in space.

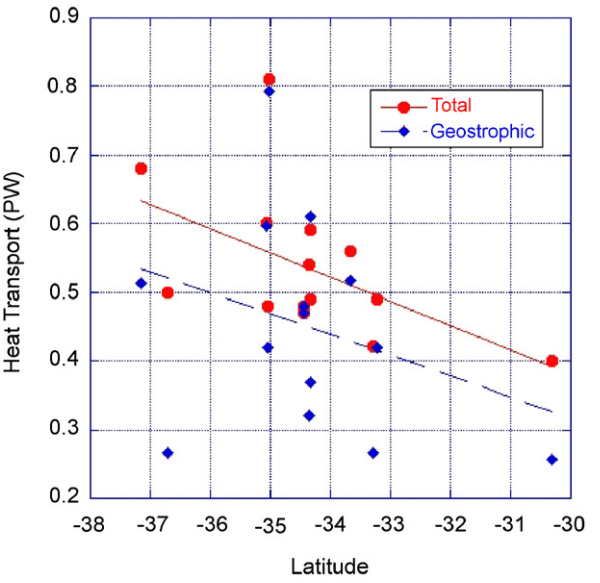

Fig. 11. Variability with latitude of the computed total (red) and geostrophic (blue) fluxes. The lines are the linear fit between the total heat transport (red) and geostrophic heat transport (blue) with latitude.

The possibility of an annual cycle is analyzed in Fig. 12. The total heat transport shows apparent interannual variability, but does not show a strong indication of seasonality (Fig. 12a). The percentage of variance explained by an annual cycle fit to the total transport is 24%, a value similar to those observed in the Parallel Ocean Climate Model (POCM) analyzed by Baringer and Garzoli (2007), 31% at 30°S and 17% at 35°S. The scatter about the annual cycle fit is in some cases natural interannual variability, and in others is due to the difference in the cruise tracks. For example, the results from the two cruises conducted during the months of July

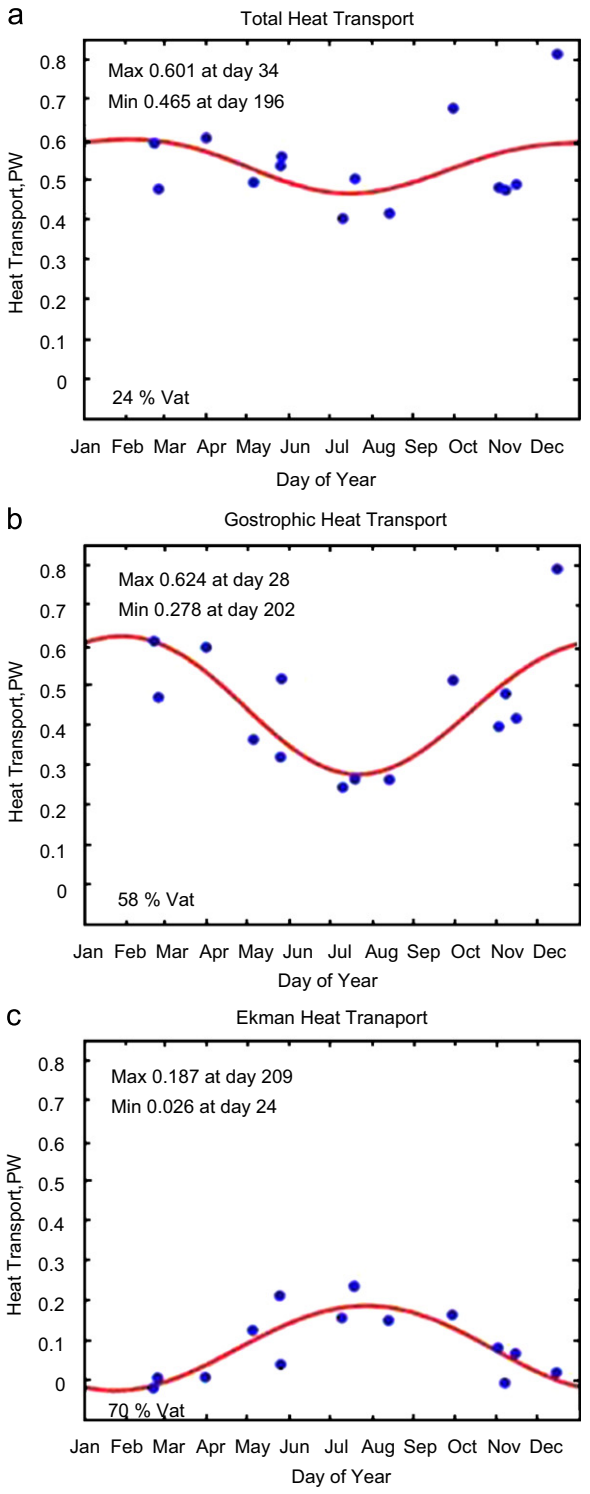

Fig. 12. Annual cycle of (a) total heat transport, (b) geostrophic heat transport and (c) Ekman heat transport.

2002 and July 2004 yield values of 0.40 and 0.50 PW, respectively. In this case, the difference is likely due to the different wind stress because the July 2002 cruise was conducted at a mean latitude of 30°19′S, where the Ekman component of the flux is low (0.16 PW), while the 2004 cruise was conducted at a mean latitude of 36°42′S, where the Ekman component of the flux is high (0.24 PW) (Tables 1 and 2 and Fig. 5). If only the geostrophic component of the flow is analyzed (Fig. 12b), minimum values of the heat transport are observed for the period July to September (around day 200). In other words, the geostrophic component of the heat transport reaches its lowest values during the austral winter when the Malvinas Current reaches its northernmost latitude. There is only a slight indication that the values are higher during the austral summer (January, February and March) when the Brazil current reaches its southern extension. The heat transport obtained from the POCM (Baringer and Garzoli, 2007) contains a seasonal cycle similar to the one observed in the Ekman transports (same amplitude and phase). This indicates that in the model, most of the variability is due to Ekman flow, while the data analysis performed in this paper suggests that the geostrophic component of the flux is an important component of the total flux.

The maximum observed value for heat transport is obtained during the month of December 2004, 0.81 PW, and it is mostly due to the geostrophic component (0.79 PW, Table 2). Average SST anomalies during the cruise indicate a warm anomaly at the eastern boundary (+5 °C). The vertical temperature profiles (not shown) indicate anomalously warm waters between 40° and 50°W extending from 100 to 500 m (with respect to climatology). These results may explain the wide range of values obtained for heat transport in the South Atlantic, as described in the introduction. Interesting to note is that if the heat transport value obtained from the data collected during December 2004 (0.81 PW) is discarded, there is a significant correlation between the total heat transport and the Brazil Current volume transport ($R = 0.43$, not shown). The relation indicates that as the southward flow from the Brazil Current intensifies, the total northward heat transport decreases. When the results from the December 2004 section are added, the correlation is destroyed ($R = 0.04$). A careful analysis of the data and procedures used to obtain the estimate for the heat transport using data

collected during the December 2004 cruise did not provide any reason to eliminate the observation.

The Ekman component of the heat flux has a marked seasonal signal that follows the variability of the wind stress in the region, with an amplitude of up to 0.2 PW (Fig. 12c). This seasonality has an sign opposite that the geostrophic component of the flow (Fig. 12b) that follows the seasonality of the Confluence Front, whose maximum amplitude has been estimated to be 0.3 PW. As a consequence, the total heat transport shows a small indication of a seasonal cycle whose amplitude is within the limits of the errors (Fig. 12a). Therefore, because of the variability of the Ekman fluxes with latitude and month (Fig. 4), direct estimates of the heat flux may vary up to 0.3 PW. The time of the year when the observations are collected may also explain difference in results obtained from direct observations due to the seasonality of the geostrophic flow in the western boundary.

The volume transports obtained in this paper east of 3°E yield a mean value of 23 Sv with a standard

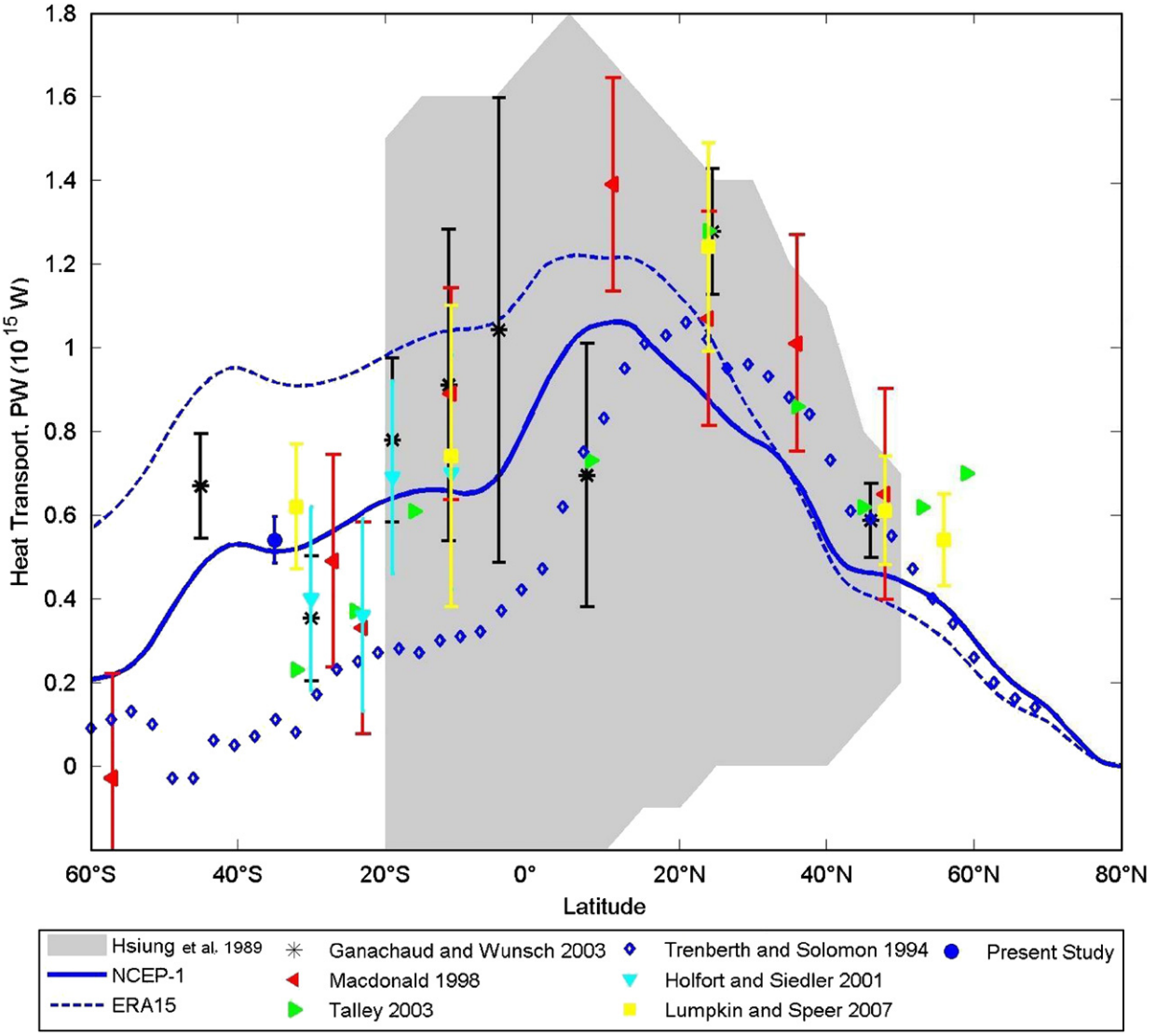

Fig. 13. Oceanic heat transport implied from integrating air-sea flux products (NCEP-1 and ERA15) starting from North Atlantic compare to several direct estimates of the heat transport from trans-basin sections (see legend). The AX18 mean heat transport (blue circle) compares favorably with the NCEP surface fluxes. The NCEP-1 annual mean was obtained from an average climatology of the years 1949–2003 (Kalnay et al., 1996). The ERA15 annual mean was derived from the ECMWF climatology based on 1979–1993 (Gibson et al., 1997) (see also Holfort and Siedler, 2001; Hsiung et al., 1989).

deviation of ±4 Sv. The presence of ring corridor (Garzoli and Gordon, 1996) raises the issue of the contribution of the rings (which are transient features) to the northward heat flux. The analysis of a high-resolution numerical model (Treguier et al., 2002) indicated that the transient eddy flux is a significant contribution to the volume transport. In Part I of this paper (Baringer and Garzoli, 2007) an estimate of the non-Ekman ageostrophic component of the flow was obtained, (0.05 PW) using the product of a general circulation model. This value was similar to previous estimates of heat transported by Agulhas rings obtained by Garzoli et al. (1999) and Goñi et al. (1997).

To put the results from this analysis into context, our results are compared to the mean value of the heat transport obtained from air–sea flux values in the Atlantic Ocean. Integrated air–sea flux values calculated (starting at in the North Atlantic) from the Atlantic Ocean reanalysis from NCEP-1 (Kalnay et al., 1996) and ERA15 (Gibson et al., 1997) models are shown in Fig. 13. Also shown in Fig. 13 are several estimates of the heat transport obtained from the literature. Estimates of the total integrated heat flux obtained as the residual calculations from air–sea fluxes from the Atlantic Ocean reanalysis from NCEP-1 and ERA15 models (Fig. 13) differs at 30°S by 0.4 PW. Therefore, estimates from air–sea fluxes will strongly depend on the products used.

The heat transport obtained in this paper at a nominal latitude of 35°S (0.54 ± 0.11 PW) is similar within the limits of the errors to those obtained by Ganachaud and Wunsch (2003) for the WOCE line A10 (30°S), 0.40 PW, using an inverse model; by Donners and Drijfhout (2004) using a numerical model at 32.5°S, 0.63 PW, and to direct calculations from the model velocity fields (Matano, personal communication) at 35°S, 0.55 PW. These values are all larger than those obtained by McDonagh and King (2005) 0.22 ± 0.08 PW across A10 using Hellerman and Rosenstein winds. It must be noticed that the authors indicate that they also obtained lower values for the WOCE line A11 (nominally 40°S), (0.43 ± 0.08 PW) than previous estimates of northward heat flux at A11 by Saunders and King (1995), 0.8 PW and Ganachaud (2003) 0.66 ± 0.12 PW, values that are closer to the estimates of this paper and the ones obtained by Lumpkin and Speer (2007) also for A11, 0.60 ± 0.08 PW.

Many of the inverse model calculations use annual mean winds to estimate the Ekman fluxes. These will provide another explanation of the differences obtained between these values and those obtained from direct observations using monthly winds. Numerical models also use different wind forcing and hence the South Atlantic heat transport obtained from these models may similarly differ.

Given the large seasonal and interannual variability, the huge influence of the variable wind field, and the different latitudes of the sections, many more observations would be needed to assess the seasonal cycle much less any climate trend from these observations. The high-density lines AX18 are to be continued at the rate of 4 per year. After a sufficient number of realizations, it is assumed that these heat transport estimates will become more robust. It is concluded that at these latitudes, the mean heat transport observed was 0.54 PW with an uncertainty of 0.18 PW.

Acknowledgments

We are very thankful for the support of Ms. Qi Yao, for the quality control of the XBT data and calculations used in this paper. Lt. Cmdrs Ariel Troisi and Fabian Vettere collected the data along the AX18 transect. Robert Roddy managed the logistics and operations for these cruises. Dr. Carlisle Thacker provided the T/S relations for the region. Dr. Gustavo Goni and Pedro DiNezio provided the satellite figures. Roberta Lusic prepared the manuscript for publication. SST anomalies are courtesy of http://cwcaribbean.aoml.noaa.gov/. We are indebted to all of them for their collaboration and support of this program. This work would not have been possible except for the hospitality of the Maersk Company, the many captains and crews of the merchant vessels Justice Container, Maersk Hong Kong, Ever Genius, and especially the Ever Garden. Funding was provided by the Office of Climate Observations and the National Oceanic and Atmospheric Administration.

References

Baringer, O.M., Garzoli, S.L., 2007. Meridional Heat Transport determined with Expendable Bathythermographs. Part 1: error estimates. Deep-Sea Research I, this issue, doi:10.1016/j.dsr.2007.03.011.

Boyer, T., Levitus, S., Garcia, H., Locarnini, R., Stephens, C., Antonov, J., 2006. Objective analyses of annual, seasonal and monthly temperature and salinity for the World Ocean on a 1/4 degree grid. International Journal of Climatology 25, 931–945.

Coachman, L.K., Aagaard, K., 1988. Transports through Bering Strait: annual and interannual variability. Journal of Geophysical Research 93, 15535–15539.

de las Heras, M.M., Schlitzer, R., 1999. On the importance of intermediate water flows for the global ocean overturning. Journal of Geophysical Research 104, 15515–15536.

de Ruijter, W.P.M., Campos, E.J.D., Cunningham, S.A., Donners, J., Gordon, A.L., Lutjeharms, J.R.E., Matano, R.P., Nof, D., Piola, A.R., 2004. The role of the South Atlantic and inter-ocean exchanges on the thermohaline circulation. First International Clivar Science Conference, Baltimore, MD.

Donners, J., Drijfhout, S.S., 2004. The Lagrangian view of South Atlantic interocean exchange in a global ocean model compared with inverse model results. Journal of Physical Oceanography 34, 1019–1035.

Duncombe Rae, C., Garzoli, S.L., Gordon, A., 1996. The eddy field of the southeast Atlantic Ocean: a statistical census from the Benguela Sources and Transport project. Journal of Geophysical Research 101, 11,949–11,964.

Flood, R.D., Shore, A.N., 1988. Mud waves in the Argentine basin and their relationship to regional bottom circulation patterns. Deep-Sea Research 35, 943–971.

Fu, L.L., 1981. The general circulation and meridional heat transport of the subtropical South Atlantic determined by inverse methods. Journal of Physical Oceanography 11, 1171–1193.

Ganachaud, A., 2003. Large-scale mass transports, water mass formation, and diffusivities estimated from World Ocean Circulation Experiment (WOCE) hydrographic data. Journal of Geophysical Research 108, 148–227.

Ganachaud, A.S., Wunsch, C., 2003. Large-scale ocean heat and freshwater transports during the World Ocean Circulation Experiment. Journal of Climate 16, 696–705.

Garzoli, S.L., 1993. Geostrophic velocity and transport variability in the Brazil–Malvinas Confluence. Deep-Sea Research I 40, 1379–1403.

Garzoli, S.L., Bianchi, A., 1987. Time-space variability of the local dynamics of the Malvinas–Brazil confluence as revealed by inverted echo sounders. Journal of Geophysical Research 92, 1914–1922.

Garzoli, S.L., Garraffo, Z., 1989. Transports, frontal motions and eddies at the Brazil–Malvinas currents confluence. Deep-Sea Research 36, 681–703.

Garzoli, S.L., Giulivi, C., 1994. What forces the variability of the southwestern Atlantic boundary currents. Deep-Sea Research I 41, 1527–1550.

Garzoli, S.L., Gordon, A.L., 1996. Origins and variability of the Benguela current. Journal of Geophysical Research 101, 897–906.

Garzoli, S.L., Richardson, P.L., Duncombe Rae, C.M., Fratantoni, D.M., Goni, G.J., Roubicek, A.J., 1999. Three Agulhas rings observed during the Benguela current experiment. Journal of Geophysical Research 104, 20971–20985.

Garzoli, S.L., Garraffo, Z., Podesta, G., Brown, O., 1992. Analysis of a general circulation model product. 1. Frontal systems in the Brazil/Malvinas and Kuroshio/Oyashio regions. Journal of Geophysical Research 97, 20117–20138.

Gibson, J., Kohlberg, P., Uppala, S., Hernandez, A., Nomura, A., Serrano, E., 1997. Era description. In: Technical Report 1, European Center for Medium-Range Weather Forecasts.

Goñi, G.J., Garzoli, S.L., Roubicek, S.L., Olson, A.J., Brown, D.B., 1997. Agulhas ring dynamics from TOPEX/POSEIDON satellite altimeter data. Journal of Marine Research 55, 861–883.

Goñi, G.J., Wainer, I., 2001. Investigation of the Brazil current front variability from altimeter data. Journal of Marine Research 106, 31,117–31,128.

Gordon, A.L., Greengrove, C.L., 1986. Geostrophic circulation of the Brazil–Falkland confluence. Deep-Sea Research 33, 573–585.

Gordon, A.L., Weiss, R.F., Smethie Jr., W.M., Warner, M.J., 1992. Thermocline and intermediate water communication between the South Atlantic and Indian Oceans. Journal of Geophysical Research 97, 7223–7240.

Hellerman, S., Rosenstein, M., 1983. Normal monthly wind stress over the World Ocean with error estimates. Journal of Physical Oceanography 13, 1093–1104.

Hogg, N., Biscayne, P., Gardner, W., Schmitz Jr., W.J., 1982. On the transport and modification of Antartic bottom water in the Vema channel. Journal of Marine Research 40, 231–263 supplement.

Holfort, J., Siedler, G., 2001. The Meridional oceanic transports of heat and nutrients in the South Atlantic. Journal of Physical Oceanography 31, 5–29.

Hsiung, J., Newelland, R.E., Houghtby, T., 1989. The annual cycle of oceanic heat—storage and oceanic meridional heat—transport. Quarterly Journal of the Royal Meteorological Society 115 (485), 1–28 Part A.

Kalnay, E., Kanamitsu, M., Kistler, R., Collins, W., Deaven, D., Gandin, L., Iredell, M., Saha, S., White, G., Woollen, J., Zhu, Y., Leetmaa, A., Reynolds, B., Chelliah, M., Ebisuzaki, W., Higgins, J., Janowiak, K.M., Ropelewski, C., Wang, J., Jenne, R., Joseph, D., 1996. In: the ncepSolncar 40-year reanalysis project. Bulletin of the American Meteorological Society 77, 437–472.

Lumpkin, R., Speer, K., 2007. Global Ocean Meridional Overturning. Journal of Physical Oceanography, in press.

Lutjeharms, J.R.E., van Ballegooyen, R.C.A., 1988. Anomalous upstream retroflection in the Agulhas current. Science 240, 1770–1772.

Macdonald, A.M., 1998. The global ocean circulation: a hydrographic estimate and regional analysis. Progress in Oceanography 41, 281–382.

Macdonald, A.M., Baringer, M.O., Ganachaud, A., 2001. Heat transport and climate. In: Steele, J.H., Thorpe, S.A., Turekian, K.K. (Eds.), Encyclopedia of Ocean Sciences, Vol. 2. London, UK, Academic Press, pp. 1195–1206.

Matano, R.P., Philander, S.G.H., 1993. Heat and mass balances of the South Atlantic Ocean calculated from a numerical model. Journal of Geophysical Research 98, 977–984.

Matano, R.P., Schlax, M.G., Chelton, D.B., 1993. Seasonal variability in the southwestern Atlantic. Journal of Geophysical Research 98, 18027–18035.

McCartney, M.S., Curry, R.A., 1993. Transequatorial flow of Antarctic bottom water in the Western Atlantic Ocean: abyssal geostrophy at the equator. Journal of Physical Oceanography 23, 1264–1276.

McDonagh, E.L., King, B.A., 2005. Oceanic fluxes in the South Atlantic. Journal of Physical Oceanography 35, 109–122.

Olson, D.B., Podesta, G.P., Evans, R.H., Brown, O.B., 1988. Temporal variations in the separation of Brazil and

Malvinas currents. Oceanography Research Paper 35, 1971–1990.

Peterson, R.G., 1992. The boundary currents in the western Argentine basin. Deep-Sea Research 39, 623–644.

Peterson, R.G., Stramma, L., 1991. Upper-level circulation in the South Atlantic Ocean. Progress in Oceanography 26, 1–73.

Piola, A.R., Gordon, A., 1989. Intermediate waters in the southwest South Atlantic. Deep-Sea Research 36, 1–16.

Richardson, P.L., Garzoli, S.L., 2003. Characteristics of intermediate water flow in the Benguela current as measured with RAFOS floats. Deep-Sea Research II 50 (1), 87–118.

Rintoul, S.R., 1991. South Atlantic interbasin exchange. Journal of Geophysical Research 96, 2675–2692.

Saunders, P.M., King, B.A., 1995. Oceanic fluxes on the WOCE A11 section. Journal of Physical Oceanography 25, 1942–1958.

Saunders, P.M., Thompson, S.R., 1993. Transport, heat, and freshwater fluxes within a diagnostic numerical model (FRAM). Journal of Physical Oceanography 23, 452–464.

Shannon, L.V., 1985. The Benguela Ecosystem, I., evolution of the Benguela, physical features and processes. Oceanography and Marine Biology 23, 105–182.

Shannon, L.V., Lutjeharms, J.R.E., Agenbag, J.J., 1989. Episodic input of Subantarctic water into the Benguela region. South African Journal of Science 85, 317–322.

Stramma, L., England, M., 1999. On the water masses and mean circulation of the South Atlantic Ocean. Journal of Geophysical Research 104, 20863–20883.

Stramma, L., Peterson, R.G., 1989. Geostrophic transport in the Benguela current region. Journal of Physical Oceanography 19, 1440–1448.

Stramma, L., Peterson, R.G., 1990. The South Atlantic current. Journal of Physical Oceanography 20, 846–859.

Talley, L.D., 2003. Shallow, intermediate, and deep overturning components of the global heat budget. Journal of Physical Oceanography 33, 530–560.

Thacker, W.C., 2007. Estimating salinity to complement observed temperature: Part 1: Gulf of Mexico. Journal of Marine Science 65/1–4, 224–248.

Treguier, A.M., Boebel, O., Barnier, B., Madec, G., 2002. Afulhas eddy fluxes in a 1/6° Atlantic model. Deep-Sea Research II 50, 251–280.

Trenberth, K.E., Solomon, A., 1994. The global heat balance: heat transport in the atmosphere and ocean. Climate Dynamics 10 (3), 107–134.

Vivier, F., Provost, C., Meredith, M.P., 2001. Remote and local forcing in the Brazil–Malvinas Region. Journal of Physical Oceanography 31, 892–913.

Zenk, W., Siedler, G., Lenz, B., Hogg, N.G., 1999. Antarctic bottom water flow through the Hunter channel. Journal of Physical Oceanography 29, 2785–2801.